PCCP

PAPER

View Article Online
View Journal | View Issue

Cite this: *Phys. Chem. Chem. Phys.*, 2025, **27**, 21458

Unveiling the molecular features of p- and n-doped polyfluorene

Andrés Felipe Quintero-Jaime,[ac] Francisco Huerta[b] and Francisco Montilla *[a]

Received 22nd May 2025,
Accepted 14th September 2025

DOI: 10.1039/d5cp01933h

rsc.li/pccp

The electrochemical doping processes of poly(9,9-dioctylfluorene) (PFO) films have been studied by a combination of vibrational and electronic spectroscopy with electrochemical methods in acetonitrile. This analysis provided a comprehensive understanding of the distinct mechanisms governing p- and n-doping and revealed the molecular nature of their respective charge carriers. P-doping induces substantial structural and optical transformations, including the formation of polaronic and quinoid domains, and is accompanied by strong interactions between the polymer and solvent molecules. In contrast, n-doping shows lower solvent interaction, faster charge equilibration, and limited structural reorganization. A key finding is that polaron compression phenomena occur exclusively under p-doping, due to inter-polaron interactions at higher doping levels. These results reveal the asymmetric roles of solvent and charge compensation in the two doping regimes and contribute to a deeper understanding of the electronic, structural, and dynamic behavior of PFO during reversible electrochemical doping.

1. Introduction

Organic conjugated polymers (CPs) have gathered significant attention in the scientific community due to their unique combination of physicochemical properties. Most of these properties arise from their ability to be chemically doped *via* mechanisms fundamentally different from those in inorganic semiconductors.[1] Doping of CPs can be carried out by either oxidation (p-doping) or reduction (n-doping) of the backbone chain. This ability enables their applications in charge-storage devices, electrochemically-gated transistors, smart windows or (electro)chemical sensors, among others.[2–4]

Doping induces localized structural distortions along the polymer backbone, favoring transformation from aromatic structures to quinoid configurations, which appear delocalized along several monomer units.[5] Electronic charges coupled with conformational lattice deformations are known as polarons. At increasing doping levels, polarons interact between themselves producing compressed polarons and, finally, bipolaronic moieties. Bipolarons, traditionally defined as pairs of like charges, are associated with a pronounced local lattice distortion.[6] However, the classical bipolaron model has been challenged.[7,8] Contemporary models (particularly those based on the oligomer approach) offer an alternative explanation for the behavior of CPs at high doping levels, conceptualizing bipolarons not as distinct entities, but as two closely interacting polarons with a singlet ground state, *i.e.* polaron pairs.[9,10]

P-doped polymers are more commonly studied and employed since they offer greater stability compared to n-doped.[11] P-doping occurs at relatively low anodic potentials, lying within the electrochemical stability window of conventional solvents and those p-polarons have been well-characterized using spectroelectrochemical techniques.[12,13] In contrast, n-doping remains far more challenging. Reduction processes require highly negative potential, often exceeding the cathodic stability of solvents, which can trigger decomposition. Furthermore, n-doped states are highly reactive, complicating both experimental analysis and practical applications.[14,15] Recent research is focused on stabilizing n-doped CPs through molecular design, air-stable dopants and tailored electrolytes to restrain degradation.[16–18]

Electrochemical doping alters the microstructure and morphology of CPs, since counterions (and solvent molecules) are incorporated in the polymer matrix to maintain the electroneutrality of the material. The uptake of ionic species and solvent, leads to a volumetric expansion of the polymer, known as swelling. In this context, closely associated with the doping process, an intriguing phenomenon is observed during the electrochemical charging and discharging of CPs. Usually, the first voltammetric cycle for doping differs in shape and peak position from successive. This phenomenon is known as slow relaxation or memory effect and has been observed in a wide variety of conducting polymers.[19,20] Several mechanisms have

[a] *Departamento de Química Física and Instituto Universitario de Materiales, Universidad de Alicante, Ap. 99, 03080, Alicante, Spain. E-mail: francisco.montilla@ua.es*
[b] *Departamento de Ingeniería Textil y Papelera, Universitat Politècnica de València, Plaza Ferrándiz y Carbonell, 1. E-03801 Alcoy, Spain*
[c] *Bernal Institute and Department of Chemical Sciences, School of Natural Sciences, University of Limerick (UL), V94 T9PX, Limerick, Ireland*

been proposed to explain the phenomenon, as those described by Malinauskas, Holze or Inzelt, among others.[21–23] One of the most accurate models is the electrochemically stimulated conformational relaxation (ESCR),[24] which considers that the charging process leads to chain rearrangement through the incorporation of counterions, while undoping results in the expulsion of those counterions from already opened channels,[25,26] following a slow close of those channels during the removal of residual solvent.[27]

The aim of the present contribution is to investigate the reversible electrochemical doping of poly(9,9-dioctylfluorene) (PFO) thin films under both p- and n-doping conditions using *in situ* UV-vis and FTIR spectroscopies. Polyfluorenes constitute a prominent class of conjugated polymers, which are widely used in organic light-emitting diodes due to their exceptional photoluminescence efficiency, high charge transport capabilities and tunable crystalline structure.[28] The study focuses on understanding the differences in relaxation behavior and charge equilibration dynamics between both doping regimes, as well as the structural and electronic transformations induced during the doping processes. Spectroelectrochemical techniques are employed to elucidate the role of solvent dynamics, polaron and bipolaron formation and changes in aromatic and quinoid domains, providing deeper knowledge of the distinct mechanisms governing p- and n-doping in PFO.

2. Experimental part

Poly(9,9-dioctylfluorene), PFO, was purchased from American Dye Source-ADS (average M_n 25 000–150 000). Anhydrous acetonitrile (≥99.8%), chloroform (≥99.9%), tetrabutylammonium hexafluorophosphate (TBA-FP, ≥99%) and ferrocene (Fc, ≥97%) were supplied by Sigma-Aldrich.

Different working electrodes were employed for electrochemical characterization. Indium tin oxide (ITO)-coated glass substrates (ITO-SOL 30, 25–35 Ω) were provided by SOLEMS. Additionally, a transparent Au-glass wafer was fabricated by sputtering gold (conditions: 50 mm separation distance to the target, 15 mA, 50 seconds at 0.05 mbar) in a metal vaporization (Balzers SCD004). Prior to its use, these electrodes were degreased with acetone under ultrasonic bath for 15 min.

Additionally, platinum and gold polycrystalline disc electrodes (geometric area 0.8 cm^2) were used as working electrodes. The cleaning procedure of metallic working electrodes comprises a polishing step with 0.05 μm Al_2O_3 slurry, followed by a rinsing with abundant water and a final thermal treatment was performed to homogenize the electrode surface and remove contaminants from the electrode surface. After the cleaning procedure, the working electrodes were modified with PFO films obtained by casting 10 μL of 1 mg mL^{-1} of PFO solution in chloroform onto the electrode surface, letting dry the solvent at room temperature.

Electrochemical studies were carried out using an eDAQ Potentiostat (EA163 model) coupled to a wave generator (EG&G Parc Model 175) and the data acquisition was done with an eDAQ e-corder 410 unit (Chart and Scope Software), using a standard three-electrode cell configuration.

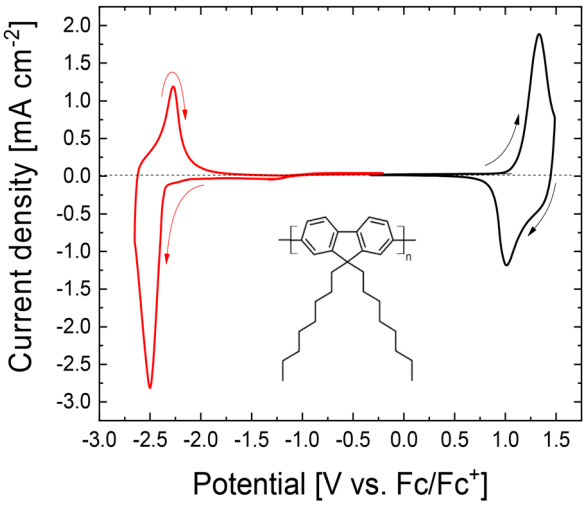

Fig. 1 Stabilized cyclic voltammetry of PFO thin film on platinum (black line) and gold (red line) electrodes during p- and n-doping, respectively. Conditions: 0.1 M TBA-FP/CH_3CN at 100 mV s^{-1} under N_2 atmosphere.

The PFO thin films deposited onto working electrodes were immersed in organic electrolyte (0.1 M TBA-FP in CH_3CN), using a platinum coil-wire as counter electrode (CE) and an Ag wire as pseudo-reference electrode, both protected by a glass capillary tube and immersed in the same electrolyte employed. The reference electrode was calibrated using the ferrocene/ferrocenium redox couple (Fc/Fc^+) added in the same solution. Nitrogen flow was maintained during all the experiments to avoid interference of O_2.

In situ UV-vis spectra were acquired using an Ocean Optics spectrophotometer (Flame model Avantes DH-2000-S and optical fibers Ocean Optics QP100-2-UV/VIS GF052107-101). Potentiostatic polarization of the modified PFO thin films were performed using a Dropsens potentiostat μSTAT 400 from the semiconductive state to the different doped states of the polymer. These experiments were carried out in a 1-cm optical path quartz cuvette making use of a PFO on either ITO or transparent Au-glass electrode.

In situ Fourier-transform infrared (FTIR) spectroscopy experiments were performed in a Nicolet 5700 spectrometer equipped with a mercury cadmium telluride (MCT) detector cooled with liquid nitrogen. The spectroelectrochemical cell with an external reflection configuration[29] was provided with a prismatic CaF_2 window beveled at 60°. Mirror-polished platinum and gold disc electrodes modified with PFO films were employed as working electrodes in these experiments and were pressed against the prismatic window to conform the thin-layer configuration.

FTIR spectra were expressed in the usual form as the normalized difference between the sample spectrum (collected at the sample potential) and the reference spectrum (collected at the reference potential) $\Delta R/R$. In these conditions, the negatively oriented absorption bands (downwards) were displayed when vibrational modes appeared or intensified at the

sample potential. On the contrary, positively oriented absorption bands (upwards) were related to species that disappeared or became IR-inactive at the sample potential.

Ex situ FTIR spectra were collected with an ATR PRO 4X spectrophotometer equipped with an ATR accessory (iQX accessory) with a ZnSe crystal kit single reflection unit.

3. Results and discussion

3.1. Electrochemical characterization

Fig. 1 shows the stabilized cyclic voltammograms recorded for a PFO thin film cast onto the surface of either a platinum electrode (for the p-doping process, anodic branch) or a gold electrode (for n-doping, cathodic branch). The gold electrode was avoided for the p-doping due to its irreversible oxidation from 0.7 V, which may lead to anodic dissolution of the metal into the organic solvent.[30]

Like other organic conjugated semiconductors, a pristine PFO thin film can be reversibly switched to a conductive state through the injection of either positive or negative charge carriers into the backbone. The right branch of Fig. 1 shows that the oxidation onset occurs at 0.85 V during the forward scan. This potential marks the beginning of hole injection (positive charge carrier formation) within the PFO structure. The p-doping process proceeds through a well-defined anodic peak at 1.33 V, while the extraction of holes (dedoping counter-process) appears in the reverse scan, showing a reduction peak at 1.02 V. Conversely, the left branch in Fig. 1 shows that the n-doping initiates at a negative potential of −2.20 V. From this onset, the electron injection into the polymer backbone continues under a single reduction peak centered at −2.50 V. The application of potentials more positive or more negative than the limits shown in the window of Fig. 1 leads to unstable voltammetric responses, likely due to polymer degradation. The fraction of oxidized or reduced monomer units, *i.e.* polymer doping level, can be determined at each potential from the integration of the voltammogram. Fig. S1 in the SI shows the different doping level reached at each potential for both p- and n-doping processes.

Electrochemical doping processes, involving the injection of mobile charges compensated by ion migration from the electrolyte solution, significantly modify the chemical, mechanical and electronic structure of conjugated polymers. Such processes stimulate conformational changes within the polymer backbone, which result in altered optoelectronic properties.[27,31,32] Memory effects during the electrochemical doping of PFO were investigated following a specific electrochemical program: first, an equilibration period to obtain a stabilized voltammogram for the doping/dedoping processes, then a relaxation step involving the application of a constant potential in the semiconductive state for 5 min to achieve a fully undoped material and, finally, a measurement stage where the potential is swept across the same range as in the initial voltammogram. More details on this potential program are given in Scheme S1 in the SI.

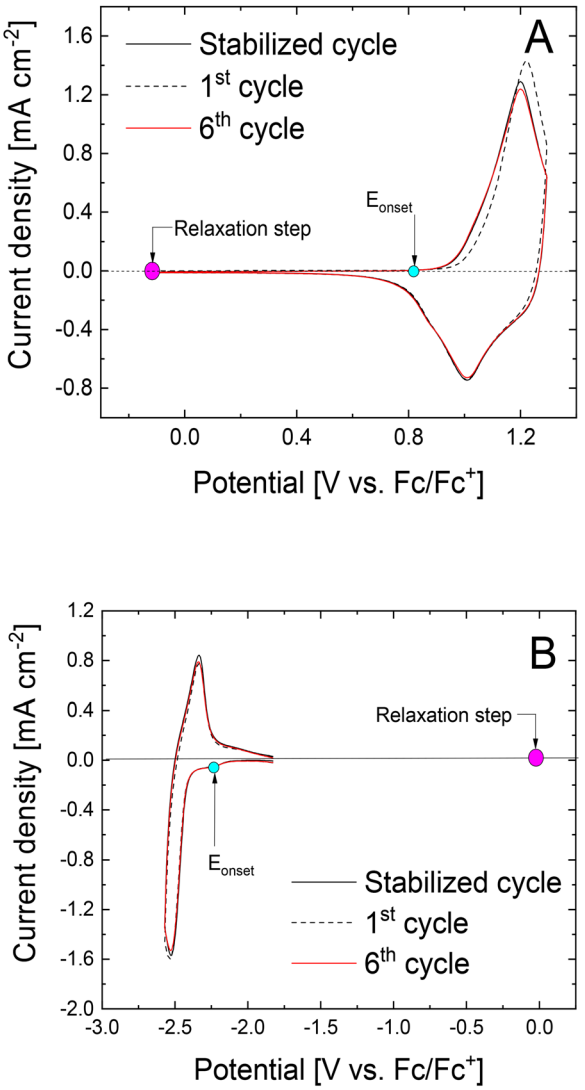

Fig. 2 Cyclic voltammograms of the first-cycle analysis for PFO thin films on Pt and Au electrodes: (A) p-doping and (B) n-doping. Conditions: 0.1 M TBA-FP/CH_3CN at 100 mV s^{-1} under N_2 atmosphere.

The p-doping process is analyzed in Fig. 2A, revealing that the curve corresponding to the first scan after the relaxation step at 0.0 V (dashed line) is shifted to higher potentials compared to the stabilized voltammogram (black solid curve). The anodic peak, appearing sharper in shape, preserves its voltammetric charge and shifts 20 mV towards higher potentials. During the six subsequent scans, the voltammogram progressively returns to a shape closely resembling that of the stabilized cycle. The positive charge injection during p-doping induces the intercalation of hexafluorophosphate anions (PF_6^-) to balance the charge, leading to polymer swelling and other transient effects through slow relaxation. This first-cycle effect is commonly observed in the electrochemical doping of conjugated polymers.

The equivalent cyclic voltammetry experiments recorded for PFO during n-doping (Fig. 2B) show no significant differences among the stabilized cycle, the first cycle after the relaxation

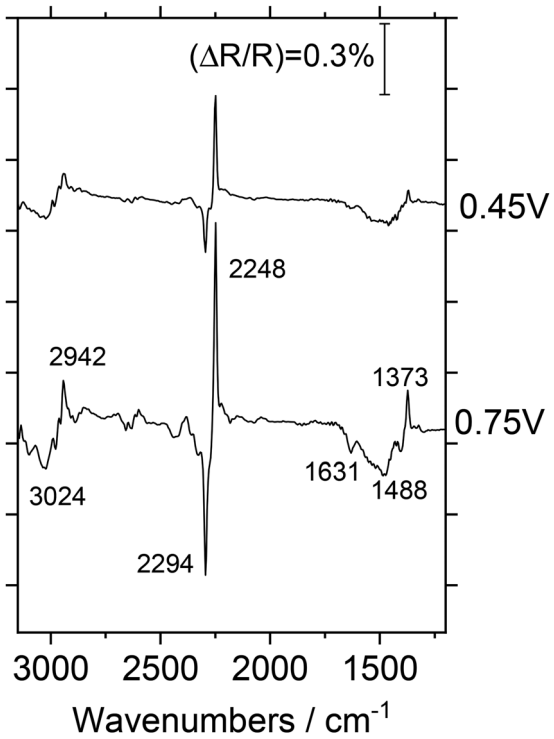

Fig. 3 *In situ* FTIR spectra for the predoping regime of a PFO thin film deposited on a Pt disk electrode in 0.1 M TBA-FP/CH_3CN. Reference potential: 0.15 V *vs.* Fc/Fc^+. Sample potentials are labeled for each spectrum. 100 interferograms at each potential.

step, and subsequent cycles. This observation is unexpected, considering that the doping process should produce negatively charged species in the polymer backbone, which would typically induce the intercalation of tetrabutylammonium cations (TBA^+) from the electrolyte. The lack of clear relaxation effects in PFO voltammograms reveals a significantly faster equilibration process for n-doping than for p-doping. This observation suggests that the solvent, or the doping ions, play different roles in the two types of doping processes.

3.2. Spectroelectrochemical characterization

Vibrational spectroscopy has been often employed for the characterization of conducting polymers, offering a more comprehensive understanding of the molecular transformations underlying the doping processes. Specifically, the analysis of PFO doping by *in situ* Fourier-Transform Infrared Spectroscopy (FTIRS) is expected to provide more detailed information about the chemical changes occurring in the polymer backbone and to shed more light on the effect of the solvent in relaxation processes. The first aim is to elucidate possible structural transformations in PFO associated with the application of positive potentials prior to the onset of p-doping. To achieve this, a reference spectrum was collected at 0.15 V to ensure that PFO was in its undoped state. Subsequently, several sample spectra were acquired at incrementally increasing potentials and, finally, these spectra were normalized to and subtracted from the reference spectrum, following the conventional form $\Delta R/R$.[33]

Fig. 3 presents two spectra obtained at sample potentials lower than the doping onset (0.45 V and 0.75 V). These spectra reveal several absorption bands related to changes occurring at the electrode–electrolyte interface.

These changes are observed in the absence of polymer redox processes, suggesting they are primarily due to modifications in the solvent-electrolyte structure, but not to the PFO itself. Specifically, negative-going bands at 1488 cm^{-1} and 3024 cm^{-1} are assigned to CH_3 group vibrational modes of acetonitrile solvent (asymmetric deformation and symmetric stretching, respectively) and positive bands at 1373 and 2942 cm^{-1} are attributed to CH_3 symmetric deformation and asymmetric stretching, respectively. The pair of intense overlapping bands emerging at 2248 cm^{-1} (upward component) and 2294 cm^{-1} (downward component) corresponds to CN stretching and some combination modes, respectively. Some of the detected bands (specifically that at 1631 cm^{-1}) may indicate the presence of water impurities in the solvent used. These assignments are summarized in Table 1.

Table 1 Proposed assignments for the *in situ* FTIR bands appearing during predoping and doping processes of PFO in CH_3CN solvent

	Frequency/cm^{-1}	Assignment	Ref.
Predoping absorptions	1373	CH_3 sym. def.	34–36
	1488	CH_3 asym. def.	
	2248	CN str.	
	2294	CH_3 def. + CC str	
	2942	CH_3 sym str.	
	3024	CH_3 asym str.	
p-doping bands	1219	C–H bend in quinoid rings	37
	1346	C–C modes quinoid–benzenoid	38
	1469	Aromatic ring C–C str.	39 and 40
	1531–1547	C═C str. in quinoid rings	37 and 41
	1608	Aromatic ring C–C bend.	40 and 42
	2923	C–H str in alkyl side chains	39
n-doping bands	1176	C–H bend in quinoid rings, C–C interring str. bipolaron	42–44
	1377	CH_3 sym. def. (CH_3CN)	34–36
	1546	C═C str. in quinoid rings	37 and 41

It is noteworthy that the intensity of all absorption bands increases proportionally with applied potential. The positive or negative character of these absorptions strongly suggests that solvent molecules undergo potential-induced diffusion or reorientation processes within the thin layer of electrolyte between the electrode surface and the CaF_2 window probed by the IR signal, facilitating the reorganization of the electrical double-layer as the potential increases. In this way, to minimize spectral interference arising from uncompensated solvent absorptions during the electrochemical injection of charge into PFO, the reference spectrum for studying the p-doping process should be acquired at the highest possible potential below the oxidation onset.

The vibrational analysis of p-doping process is presented in Fig. 4. The reference spectrum was acquired previously at 0.8 V and the sample spectra were then collected at increasing potentials beyond the oxidation onset. Fig. 4 shows in the spectrum obtained at 0.9 V, the bipolar band corresponding to the CN stretching vibration (centered around 2250 cm^{-1}) appears inverted compared to the band observed in the pre-doping regime. This inversion can be interpreted in terms of the net balance of solvent molecules at doping potentials. When PFO is electrochemically oxidized, the generated positive charge is compensated by the incorporation of PF_6^- anions into the polymer film. Simultaneously, there is an associated counter-flow of TBA^+ cations out of the electrical double layer. Both processes, which involve the movement of ions dragging a significant number of solvent molecules, dramatically modify the structure of the thin layer probed by the IR beam. In addition, the possibility of new interactions between the oxidized polymer and acetonitrile molecules cannot be ruled out. This interpretation is supported by the appearance of negative absorptions at 2942 and 1377 cm^{-1} (both bands presented an opposite character in Fig. 3) which confirms a modification in the local concentration or orientation of acetonitrile molecules during p-doping.

Regarding PFO absorption bands, Fig. 4 clearly illustrates the spectral changes as the doping level increases. First, a significant baseline deformation is observed at higher wavenumbers (>2500 cm^{-1}), which can be attributed to the appearance of broad absorption bands associated with the formation of polaronic moieties along the conjugated chains (tail of optical transition bands). On the other hand, in the lower wavenumber region, several new bands appear, revealing the formation and breaking of bonds within the polymer structure. Particularly interesting is the positive-going band at 1469 cm^{-1} which, arising at moderate potentials (0.9 V, doping level 0.005), reveals the disappearance of aromatic C–C stretching modes in fluorene units as the doping level increases. Simultaneously, the two overlapped negative-going features at 1531–1547 cm^{-1}, attributed to six-membered quinoid ring C=C vibrations, are commonly observed for other conducting polymers when aromatic modes transform into quinoid structures. The formation of quinoid domains can also be detected by a negative-going absorption at 1219 cm^{-1}, which is related to C–H bending in quinoid rings, and an additional negative feature at 1346 cm^{-1}, which, according to literature data, could be attributed to C–C modes linking phenyl units in the boundary fragment between benzenoid and quinoid structures. Such an absorption appears partially overlapped by uncompensated solvent CH absorptions. It is important to acknowledge the uncertainty surrounding the assignment of the absorption band at 1423 cm^{-1}. This ambiguity arises from the fact that multiple components in the system (namely, the solvent,

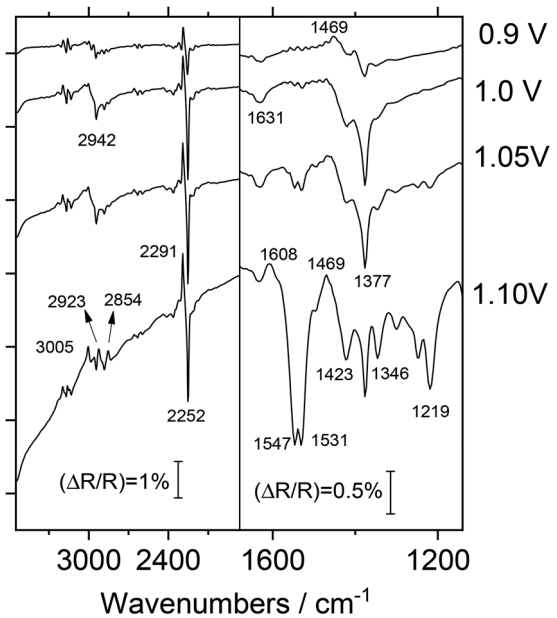

Fig. 4 *In situ* FTIR spectra collected during the p-doping process of a PFO thin film deposited on a Pt disk electrode in 0.1 M TBA-FP/CH_3CN. Reference potential: 0.85 V *vs.* Fc/Fc^+. Sample potential labeled for each spectrum. 100 interferograms at each potential.

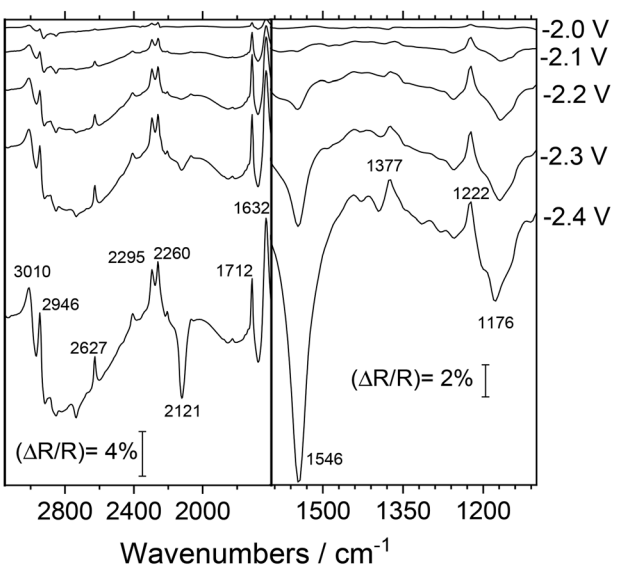

Fig. 5 *In situ* FTIR spectra collected during the n-doping of PFO thin film deposited on Au disk electrode in 0.1 M TBA-FP/CH_3CN. Reference potential: −1.7 V *vs.* Fc/Fc^+. Sample potential labeled for each spectrum. 100 interferograms at each potential.

electrolyte and polymer) all exhibit *ex situ* FTIR bands within this specific frequency range (see Fig. S2–S4 in the SI). Consequently, attributing this absorption to a single vibrational mode becomes challenging without complementary analytical techniques.

An additional set of experiments was conducted to study the absorption bands generated during the sweep towards more negative potential (n-doping), with results shown in Fig. 5. In this case, the reference spectrum was acquired at −1.7 V where no faradaic response of the polymer layer occurs. Before reaching the n-doped state of the polymer (at sample potentials of −2.0 and −2.1 V, doping level 0.002 and 0.004, respectively) a series of positive-going features appear.

Absorptions at 2291 and 2252 cm^{-1} related to CN stretching, were already visible. Besides, two more positive bands appear at 2946 and 1631 cm^{-1}, attributed to acetonitrile methyl modes and the presence of minor water impurities, respectively. In this case, it seems that the solvent molecules are expelled when the electrode is polarized negatively.

Upon reaching the n-doping potential (−2.2 V, doping level 0.013), it is noteworthy that solvent-related bands remain unmodified, in contrast to the observations during p-doping. This suggests that the n-doped polymer does not significantly alter the orientation or distribution of solvent molecules at the electrode interface. Spectral changes directly related to n-doping include the emergence of a prominent negative-going band at 1546 cm^{-1}, revealing the formation of quinoid domains from −2.2 V (Fig. 5). The broad negative absorption at 1176 cm^{-1} is attributed to the formation of bipolaronic units within the polymer structure, which could be related to the baseline alteration recorded at frequencies above 2400 cm^{-1}, in parallel with what is observed during p-doping. The assignment of the 1222 cm^{-1} positive band at high n-doping levels remains uncertain. While clearly associated with the PFO structure, this band exclusively appears during negative-going potential excursions. A reasonable explanation involves the disappearance of a specific aromatic vibrational mode during n-bipolaron formation.

At highly negative potentials, particularly beyond −2.3 V (doping level 0.12), a new negative-going feature appears at 2117 cm^{-1}, which is tentatively attributed to CN stretching modes in cyanide species arising from the electrochemically-induced degradation of acetonitrile solvent. In addition, the positive peak at 1377 cm^{-1} may indicate the uncompensated absorption of solvent molecules resulting from polymer swelling during the n-doping process. In summary, spectroscopic results confirm that p-doping occurs mainly through the oxidation of aromatic rings, which leads to the formation of radical cations, as discussed in Fig. 4. These species can be then delocalized along adjacent rings, giving rise to quinoid structures. The formation of quinoid domains is also observed during the n-doping process.

In situ FTIR spectroscopy also reveals that the interaction between doped PFO and solvent molecules differs significantly when comparing p-doped and n-doped states. The polymer doped with positive polarons undergoes a solvation process stimulated by the interaction between its positive charge and solvent molecules, which results in a detectable change in the orientation of their active dipole moment. On the contrary, at n-doping potentials, no significant modifications in acetonitrile bands are observed, indicating negligible interaction between solvent molecules and the n-doped polymer. This minor interaction is consistent with the absence of first-cycle effects in Fig. 2B. It also reveals that, while the entry and exit of ions is driven by the electric field established by charges on the

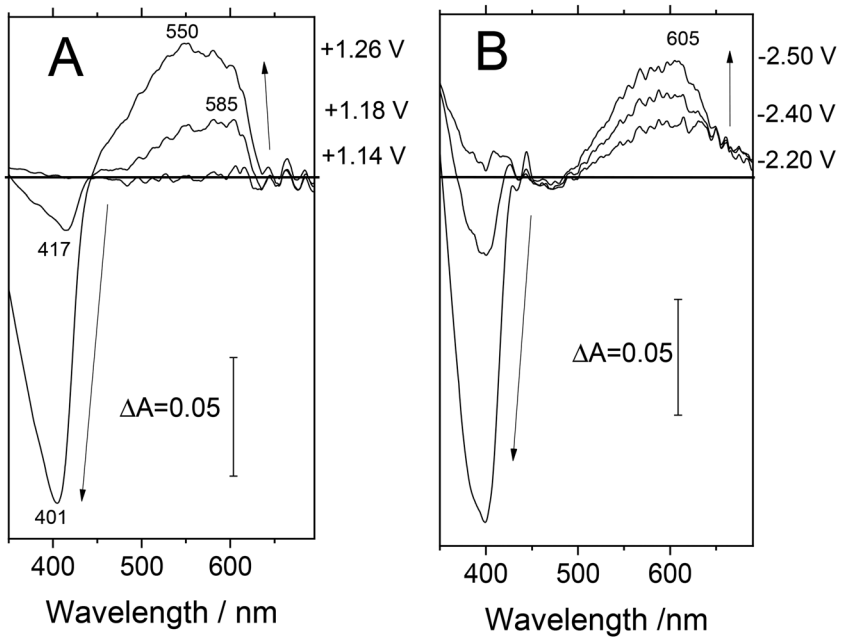

Fig. 6 *In situ* UV-vis spectra of PFO thin films recorded in 0.1 M TBA-FP/CH_3CN at different overpotentials during (A) p-doping and (B) n-doping. The initial UV-vis spectrum of PFO on ITO electrode appears in Fig. S5 in SI.

polymer chains, the movement of solvent molecules is slow and primarily governed by polymer–solvent interactions.

A deeper understanding of the transition processes in PFO from semiconductive to conductive states can be obtained using *in situ* UV-vis coupled to the electrochemical set-up. This spectro-electrochemical technique provides a real-time observation of the doping process, as new energy levels emerge in the optical bandgap when the applied potential is swept. Fig. 6 shows the recorded spectra for PFO films submitted to p- or n-doping.

The application of a potential higher than 0.85 V, the oxidation onset, to the PFO-modified electrode does not induce clear absorptions up to +1.15 V (doping level 0.22), as seen in Fig. 6A. However, from 1.15 V onwards, a negative band appears at 417 nm, corresponding to the bleaching of the characteristic $\pi\pi^*$ absorption band of the PFO neutral state, in accordance with data reported for several conjugated polymers.[45,46] Simultaneously, a positive adsorption band appears in the yellow-orange region (~585 nm) correlated with the transitions

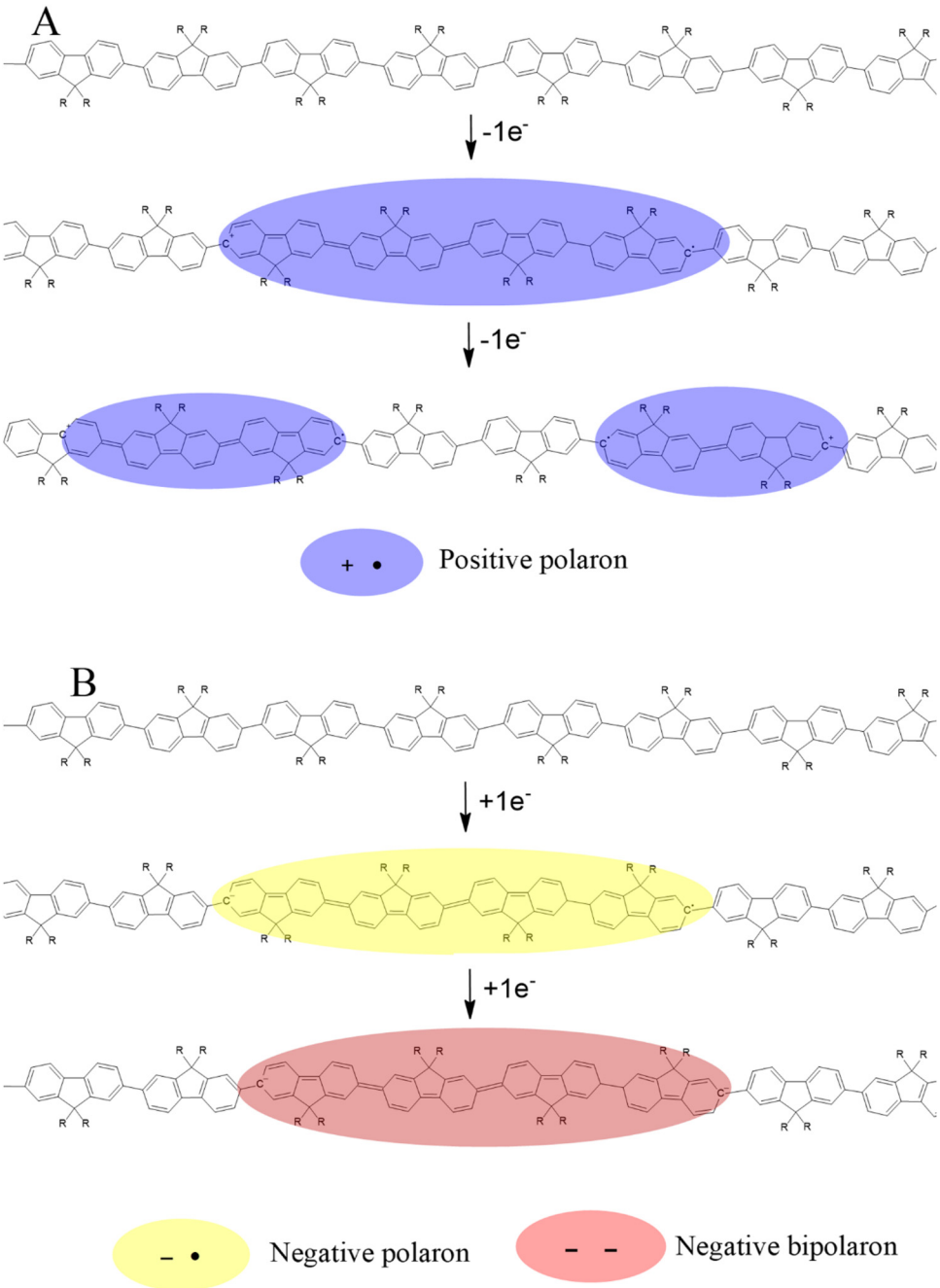

Scheme 1 Models for the p-doping and the n-doping processes in PFO compatible with the *in situ* FTIR and UV-vis spectroscopy. Delocalization of injected charge will form quinoid structures in both cases. (A) p-doping: undoped backbone → polaron → multiple (compressed) polarons (B) n-doping: undoped backbone → polaron → bipolaron.

of the electrochemically generated polaron species. The position associated to the ππ* vibronic feature of the neutral bleached blue shifts with the potential biasing until the saturation of the chromophores is reached at 1.26 V (doping level 0.44). Furthermore, the polaron band at *ca.* 550 nm is hypsochromically shifted to higher energy, a phenomenon that was associated by Takeda[47] to the confining of polaronic species and their compression in the PFO chains or to the formation of associated polarons.[45] Deeper doping levels produce an overoxidation of the PFO structure, reducing the intensity of the predominant absorption of the polaron due to the formation of bipolaronic species.[47]

During the n-doping process (Fig. 6B), features associated with the bleaching band of neutral PFO emerge near 400 nm starting from −2.20 V (doping level 0.013). The intensity of this bleaching band increases as more negative potential is applied to the polymer film. Unlike p-doping, the band position remains constant, reaching maximum intensity at −2.50 V (doping level 0.6). Applying potentials more negative than −2.50 V leads to irreversible degradation of the polymer film. In parallel to the bleaching band, a positive-going band appears at 605 nm, which can be attributed to the optical transitions of negative polarons. The intensity of this band increases as the potential is made more negative.

The blue-shift of the ππ* absorption observed during p-doping contrasts with the fixed position during n-doping. This observation strongly suggests distinct behaviors of the respective polaronic species. At low p-doping levels, the emerging positive polarons behave as nearly independent, non-interacting entities (see Scheme 1A).

However, at high doping levels increased p-polaron density enhances Coulomb-mediated interactions between adjacent charge carriers.[48] Such an interference leads to compression phenomena[10] which should precede any potential bipolaron generation, if it occurs. Conversely, the absence of a shift in the ππ* absorption suggests that emerging n-polarons (or n-bipolarons) do not undergo further evolution (Scheme 1B), which would be consistent with a lack of polaron compression at increasing doping levels.[8,10] In this context, the different role played by the solvent should not be excluded as a contributing factor.

4. Conclusions

PFO thin films can be reversibly switched to a conductive state through the injection of either positive or negative charge carriers. The electrochemical bandgap for PFO was determined to be 3.4 eV, which agrees with the optical bandgap reported in the literature. Cyclic voltammetry analysis revealed distinct relaxation behaviors for the p- and n-doping processes. The p-doping process exhibited a first-cycle effect (slow relaxation), whereas n-doping showed no significant differences between the stabilized cycle, the first cycle after the relaxation stage and subsequent cycles, suggesting faster equilibration.

In situ FTIR spectroscopy confirmed that solvent molecules undergo potential-induced diffusion processes during the predoping regime, affecting the reorganization of the electrochemical double layer. During p-doping, significant spectral changes were observed, including a distortion of the baseline, which is associated with the formation of polarons and the transformation of aromatic structures into quinoid domains. The spectral changes associated with n-doping were less pronounced, with the main features being the formation of quinoid domains and bipolaronic moieties. In addition, the orientation or distribution of solvent molecules at the electrode interface is not significantly altered under n-doping conditions, which is consistent with the absence of relaxation effects.

In situ UV-vis spectroscopy revealed the bleaching of aromatic ππ* transitions and new polaron intraband absorptions during doping, with different behavior under p- and n-doping conditions. Polaron compression as the p-doping level increases seems at the origin of the progressive band shift towards higher energies. In contrast, n-doping exhibits a more stable polaron band position throughout the doping process, which seems related to the formation of smaller effective length polarons due to the occurrence of bipolaronic moieties. The different roles played by the solvent in p-doping and n-doping processes may contribute to these differences.

Conflicts of interest

There are no conflicts to declare.

Data availability

The data supporting this article have been included as part of the SI. Data for potential program for p-doping and n-doping programs, potentiostatic polarization of PFO thin films between the undoped and doped state, FTIR-ATR spectra of different materials used in the present work are included in the supplementary information. See DOI: **https://doi.org/10.1039/d5cp01933h**.

Acknowledgements

Financial support by Spanish Ministry of Science (TED2021-129894B-I00), Generalitat Valenciana (MFA/2022/058 and CIPROM/2021/62 projects) and European Union (NextGeneration EU PRTR-C17.I1) is gratefully acknowledged.

References

1 J. Rivnay, S. Inal, A. Salleo, R. M. Owens, M. Berggren and G. G. Malliaras, Organic electrochemical transistors, *Nat. Rev. Mater.*, 2018, **3**, 1–14, DOI: **10.1038/natrevmats.2017.86**.
2 A. Facchetti, π-Conjugated polymers for organic electronics and photovoltaic cell applications, *Chem. Mater.*, 2011, **23**, 733–758, DOI: **10.1021/cm102419z**.
3 R. J. Mortimer, D. R. Rosseinsky and P. M. S. Monk, *Electrochromic Materials and Devices*, Wiley Blackwell, 2015, DOI: **10.1002/9783527679850**.

4 T. Nezakati, A. Seifalian, A. Tan and A. M. Seifalian, Conductive Polymers: Opportunities and Challenges in Biomedical Applications, *Chem. Rev.*, 2018, **118**, 6766–6843, DOI: 10.1021/acs.chemrev.6b00275.
5 R. Noriega, J. Rivnay, K. Vandewal, F. P. V. Koch, N. Stingelin, P. Smith, M. F. Toney and A. Salleo, A general relationship between disorder, aggregation and charge transport in conjugated polymers, *Nat. Mater.*, 2013, **12**, 1038–1044, DOI: 10.1038/nmat3722.
6 J. L. Bredas and G. B. Street, Polarons, Bipolarons, and Solitons in Conducting Polymers, *Acc. Chem. Res.*, 1985, **18**, 309–315.
7 F. C. Spano and C. Silva, H- and J-aggregate behavior in polymeric semiconductors, *Annu. Rev. Phys. Chem.*, 2014, **65**, 477–500, DOI: 10.1146/annurev-physchem-040513-103639.
8 Y. Furukawa, Electronic absorption and vibrational spectroscopies of conjugated conducting polymers, *J. Phys. Chem.*, 1996, **100**, 15644–15653, DOI: 10.1021/jp960608n.
9 Y. Liu, S. Gao, X. Zhang, J. H. Xin and C. Zhang, Probing the nature of charge carriers in one-dimensional conjugated polymers: a review of the theoretical models, experimental trends, and thermoelectric applications, *J. Mater. Chem. C.*, 2022, **11**, 12–47, DOI: 10.1039/d2tc03574j.
10 J. Bakalis, A. R. Cook, S. Asaoka, M. Förster, U. Scherf and J. R. Miller, Polarons, compressed polarons, and bipolarons in conjugated polymers, *J. Phys. Chem. C.*, 2014, **118**, 114–125, DOI: 10.1021/jp408910a.
11 A. J. Heeger, Semiconducting and Metallic Polymers: The Fourth Generation of Polymeric Materials, *J. Phys. Chem. B*, 2001, **105**, 8475–8491, DOI: 10.1021/jp011611w.
12 S. Garreau, G. Louarn and J. Buisson, In situ spectroelectrochemical Raman studies of poly(3,4-ethylenedioxythiophene)(PEDT), *Macromolecules*, 1999, **32**, 6807, DOI: 10.1021/ma9905674.
13 P. Damlin, C. Kvarnström, A. Petr, P. Ek, L. Dunsch and A. Ivaska, In situ resonant Raman and ESR spectroelectrochemical study of electrochemically synthesized poly(p-phenylenevinylene), *J. Solid State Electrochem.*, 2002, **6**, 291–301, DOI: 10.1007/s100080100240.
14 S. Griggs, A. Marks, H. Bristow and I. McCulloch, n-Type organic semiconducting polymers: stability limitations, design considerations and applications, *J. Mater. Chem. C.*, 2021, **9**, 8099–8128, DOI: 10.1039/d1tc02048j.
15 C. G. Tang, K. Hou and W. L. Leong, The Quest for Air Stability in Organic Semiconductors, *Chem. Mater.*, 2024, **36**, 28–53, DOI: 10.1021/acs.chemmater.3c02093.
16 Y. Chen, S. Ghosh, X. Liu, I. V. Zozoulenko, M. Fahlman and S. Braun, Experimental and Theoretical Investigation into the Polaron Structure of K-Doped Polyfluorene Films, *J. Phys. Chem. C.*, 2021, **125**, 937–945, DOI: 10.1021/acs.jpcc.0c08442.
17 J. Li, S. Deng, J. Hu and Y. Liu, Cation exchange improves the efficiency and stability of the n-doping of π-conjugated polymers, *J. Mater. Chem. A*, 2024, **12**, 21434–21441, DOI: 10.1039/d4ta03920c.
18 Y. Yamashita, S. Kohno, E. Longhi, S. Jhulki, S. Kumagai, S. Barlow, S. R. Marder, J. Takeya and S. Watanabe, N-type molecular doping of a semicrystalline conjugated polymer through cation exchange, *Commun. Mater.*, 2024, **5**, 1–7, DOI: 10.1038/s43246-024-00507-2.
19 J. Heinze, B. A. Frontana-Uribe and S. Ludwigs, Electrochemistry of Conducting Polymers-Persistent Models and New Concepts, *Chem. Rev.*, 2010, **110**, 4724–4771, DOI: 10.1021/cr900226k.
20 W. A. Marmisolle, D. Posadas and M. I. Florit, An experimental study of the intrinsic fluorescence emission and Electrochemically Induced Ageing in poly-o-methylaniline films, *Electrochim. Acta*, 2013, **109**, 894–900, DOI: 10.1016/j.electacta.2013.07.170.
21 R. Mazeikiene and A. Malinauskas, A study into electrochemical slow relaxation of polyaniline, *Synth. Met.*, 2002, **129**, 61–66.
22 E. Csahók, E. Vieil and G. Inzelt, In situ dc conductivity study of the redox transformations and relaxation of polyaniline films, *J. Electroanal. Chem.*, 2000, **482**, 168–177, DOI: 10.1016/S0022-0728(00)00044-9.
23 G. Inzelt, Conducting polymers: Past, present, future, *J. Electrochem. Sci. Eng.*, 2018, **8**, 3–37, DOI: 10.5599/jese.448.
24 T. F. Otero and I. Boyano, Comparative study of conducting polymers by the ESCR model, *J. Phys. Chem. B*, 2003, **107**, 6730–6738, DOI: 10.1021/jp027748j.
25 A. Robert Hillman, S. J. Daisley and S. Bruckenstein, Solvent effects on the electrochemical p-doping of PEDOT, *Phys. Chem. Chem. Phys.*, 2007, **9**, 2379–2388, DOI: 10.1039/b618786b.
26 F. Bonafè, C. Dong, G. G. Malliaras, T. Cramer and B. Fraboni, Subsurface Profiling of Ion Migration and Swelling in Conducting Polymer Actuators with Modulated Electrochemical Atomic Force Microscopy, *ACS Appl. Mater. Interfaces*, 2024, **16**, 36727–36734, DOI: 10.1021/acsami.4c08459.
27 F. Montilla and R. Mallavia, In situ electrochemical fluorescence studies of PPV, *J. Phys. Chem. B*, 2006, **110**, 25791–25796.
28 K. Müllen and U. Scherf, Conjugated Polymers: Where We Come From, Where We Stand, and Where We Might Go, *Macromol. Chem. Phys.*, 2023, **224**, 2200337, DOI: 10.1002/macp.202200337.
29 J. T. Li, Z. Y. Zhou, I. Broadwell and S. G. Sun, In-situ infrared spectroscopic studies of electrochemical energy conversion and storage, *Acc. Chem. Res.*, 2012, **45**, 485–494, DOI: 10.1021/ar200215t.
30 P. Jovanovič, V. S. Šelih, M. Šala and N. Hodnik, In situ electrochemical dissolution of platinum and gold in organic-based solvent, *Npj Mater. Degrad.*, 2018, **2**, 1–4, DOI: 10.1038/s41529-018-0031-8.
31 T. F. Otero, H. Grande, J. Rodriguez and A. New, Model for Electrochemical Oxidation of Polypyrrole Under Conformational Relaxation Control, *J. Electroanal. Chem.*, 1995, **394**, 211–216.
32 R. Giridharagopal, L. Q. Flagg, J. S. Harrison, M. E. Ziffer, J. Onorato, C. K. Luscombe and D. S. Ginger,

Electrochemical strain microscopy probes morphology-induced variations in ion uptake and performance in organic electrochemical transistors, *Nat. Mater.*, 2017, **16**, 737–742, DOI: 10.1038/nmat4918.

33 M. J. Sáenz-Espinar, A. F. Quintero-Jaime, A. Gamero-Quijano, F. Montilla and F. Huerta, Promotion of Direct Electron Transfer to Cytochrome *c* by Functionalized Thiophene-based Conducting Polymers, *ChemElectroChem*, 2024, **11**, e202300429, DOI: 10.1002/celc.202300429.

34 E. M. Kosower, G. Markovich and G. Borz, Thin-film infrared spectroscopy of acetonitrile, *ChemPhysChem*, 2007, **8**, 2513–2519, DOI: 10.1002/cphc.200700465.

35 Y. Koga, S. Kondo, S. Saeki and W. B. Person, Infrared intensities of acetonitrile, *J. Phys. Chem.*, 1984, **88**, 3152–3157, DOI: 10.1021/j150658a048.

36 E. L. Pace and L. J. Noe, Infrared Spectra of Acetonitrile and Acetonitrile-d3, *J. Chem. Phys.*, 1968, **49**, 5317–5325, DOI: 10.1063/1.1670050.

37 P. Damlin, C. Kvarnström and A. Ivaska, In situ external reflection Fourier transform infrared spectroscopic study on the structure of the conducting polymer poly(paraphenylene), *Analyst*, 1996, **121**, 1881–1884, DOI: 10.1039/AN9962101881.

38 V. M. Kobryanskii and S. L. Kotova, Proving the formation of quinoid fragments in vacuum deposited poly-paraphenylene films by IR-spectroscopy, *Synth. Met.*, 1997, **84**, 667–668, DOI: 10.1016/s0379-6779(96)04100-8.

39 W. Zhao, T. Cao and J. M. White, On the origin of green emission in polyfluorene polymers: The roles of thermal oxidation degradation and crosslinking, *Adv. Funct. Mater.*, 2004, **14**, 783–790, DOI: 10.1002/adfm.200305173.

40 F. Changli, X. Jingkun, C. Wen, L. Baoyang, M. Huaming, L. Congcong and L. Guodong, Polyfluorene derivatives with hydroxyl and carboxyl substitution: electrosynthesis and characterization, *J. Phys. Chem. C.*, 2009, **113**, 9900–9910, DOI: 10.1021/jp900323w.

41 M. C. Pham, S. Aeiyach, J. Moslih, P. Soubiran and P. C. Lacaze, An in-situ multiple internal reflection Fourier transform infrared spectroscopic (MIRFTIRS) investigation of the growth mechanism of polyphenylene during electrooxidation of biphenyl in methylene dichloride, *J. Electroanal. Chem.*, 1990, **277**, 327–336, DOI: 10.1016/0022-0728(90)85111-H.

42 C. G. Barbosa, D. C. Bento, L. O. Péres, G. Louarn and H. de Santana, Changes induced by electrochemical oxidation of poly(9,9-dioctylfluorene-*alt*-thiophene): towards a correlation between charge transport, molecular structure modifications and degradation, *J. Mater. Sci. Mater. Electron.*, 2016, **27**, 10259–10269, DOI: 10.1007/s10854-016-5107-z.

43 I. Orion, J. Buisson and S. Lefrant, Spectroscopic studies of polaronic and bipolaronic species in-doped poly(paraphenylenevinylene), *Phys. Rev. B: Condens. Matter Mater. Phys.*, 1998, **57**, 7050–7065, DOI: 10.1103/PhysRevB.57.7050.

44 S. Lefrant, J. P. Buisson, M. Baitoul and I. Orion, Characterization of the neutral and doped states of polyphenylenevinylene by resonance spectroscopies, *Pure Appl. Opt.*, 1996, **5**, 613–620, DOI: 10.1088/0963-9659/5/5/015.

45 F. Montilla, A. Ruseckas and I. D. W. W. Samuel, Absorption cross-sections of hole polarons in glassy and β-phase polyfluorene, *Chem. Phys. Lett.*, 2013, **585**, 133–137.

46 M. J. Bird, J. Bakalis, S. Asaoka, H. Sirringhaus and J. R. Miller, Fast Holes, Slow Electrons, and Medium Control of Polaron Size and Mobility in the DA Polymer F8BT, *J. Phys. Chem. C.*, 2017, **121**, 15597–15609, DOI: 10.1021/acs.jpcc.7b04602.

47 N. Takeda, S. Asaoka and J. R. Miller, Nature and energies of electrons and holes in a conjugated polymer, polyfluorene, *J. Am. Chem. Soc.*, 2006, **128**, 16073–16082, DOI: 10.1021/ja062596h.

48 T. Lanz, E. M. Lindh and L. Edman, On the asymmetric evolution of the optical properties of a conjugated polymer during electrochemical p- and n-type doping, *J. Mater. Chem. C*, 2017, **5**, 4706–4715, DOI: 10.1039/c7tc01022b.